PERGAMON

International Journal of Solids and Structures 40 (2003) 1165–1187

INTERNATIONAL JOURNAL OF SOLIDS and STRUCTURES

www.elsevier.com/locate/ijsolstr

A semi-analytical elastic stress–displacement solution for notched circular openings in rocks

G.E. Exadaktylos [a,*], P.A. Liolios [a], M.C. Stavropoulou [b]

[a] *Mining Engineering Design Laboratory, Department of Mineral Resources Engineering, Technical University of Crete, Akrotiri, GR-73100, Chania, Greece*

[b] *Department of Engineering Science, Section of Mechanics, National Technical University of Athens, 5 Heroes of Polytechnion Av, GR-15773 Athens, Greece*

Received 22 February 2002; received in revised form 5 November 2002

Abstract

A semi-analytical plane elasticity solution of the circular hole with diametrically opposite notches in a homogeneous and isotropic geomaterial is presented. This solution is based on: (i) the evaluation of the conformal mapping function of a hole of prescribed shape by an appropriate numerical scheme and (ii) the closed-form solutions of the Kolosov–Muskhelishvili complex potentials. For the particular case of circular notches—which resemble to the circular cavity breakout in rocks—it is demonstrated that numerical results pertaining to boundary stresses and displacements predicted by the finite differences model FLAC^{2D}, as well as previous analytical results referring to the stress-concentration-factor, are in agreement with analytical results. It is also illustrated that the solution may be easily applied to non-rounded diametrically opposite notch geometries, such as ''dog-eared'' breakouts by properly selecting the respective conformal mapping function via the methodology presented herein. By employing a stress-mean-value brittle failure criterion that takes into account the stress-gradient effect in the vicinity of the curved surfaces in rock as well as the present semi-analytical solution, it is found that a notched hole, e.g. borehole or tunnel breakout, may exhibit stable propagation. The practical significance of the proposed solution lies in the fact that it can be used as a quick-solver for back-analysis of borehole breakout images obtained in situ via a televiewer for the estimation of the orientation and magnitude of in situ stresses and of strain–stress measurements in laboratory tests.

Keywords: Notches; Conformal mapping; Plane elasticity; Complex variables; Breakouts; Boreholes

1. Introduction

Notched shaped configurations of rock cavities such as that shown in Fig. 1 are often encountered in mining, petroleum and geophysical engineering practice. They are present in deep boreholes as breakouts and in underground openings exhibiting sidewall spalling. In Fig. 1, the formation of the breakout

* Corresponding author. Tel.: +30-8210-37450/28210-37650; fax: +30-28210-69554.
E-mail address: exadakty@mred.tuc.gr (G.E. Exadaktylos).

0020-7683/02/$ - see front matter © 2002 Elsevier Science Ltd. All rights reserved.
doi:10.1016/S0020-7683(02)00646-7

Fig. 1. Underground opening exhibiting side collapse in the form of successive spalling forming a stable breakout shape.

cross-section by successive spalling can be clearly seen. Field practice shows that the geometry of such notched configurations can greatly influence the load bearing capacity of the rock structure and consequently its stability.

The excavation process reduces the confining stress to zero on the boundary of the opening. Thus, tunnel and borehole breakouts occur under high in situ stresses when the tangential stress at the excavation wall overcomes the uniaxial compressive strength of the rock. Under unequal principal stresses rock failure that is manifested by axial splitting and spalling fractures that are often extensional in nature, is observed in two diametrically opposed zones parallel to the minor principal stress forming a notched shaped excavation. An idealized breakout geometry is depicted in Fig. 2 where the initial breakout is shown by the dashed curve. Such breakouts are valuable indicators of the direction of action of the minimum compressive stress, while their size and shape, recorded via dipmeters and more precisely now by televiewers, may provide information about the magnitudes of the maximum and minimum stresses relative to the strength of the rock. As the in situ strength of rock and its state of stress are difficult to determine at great depth, observations of the size and shape of the breakouts and conditions under which they form could lead to estimation of these parameters, provided that a thorough understanding of the mechanisms involved in breakout formation become clear. According to Guisiat and Haimson (1992), Hottman et al. (1979) were perhaps the first investigators to attempt to estimate magnitudes of horizontal principal stresses from borehole breakouts. The good agreement of their estimation with other stress indicators led both Gough and Bell (1982) and

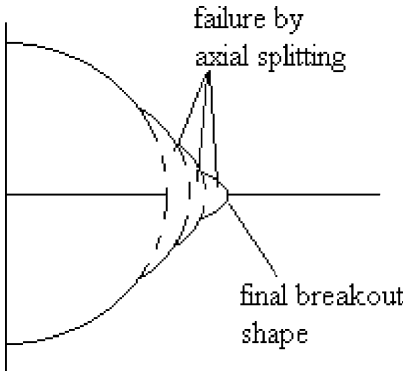

Fig. 2. Idealized breakout configuration. The initial breakout shape is rounded whereas the final cross-sectional shape of the breakout is wedge-shaped (dog-eared).

Zoback et al. (1985) to investigate the mechanisms of borehole breakouts from field and laboratory experiments. They concluded that size, shape and depth could be predicted by using Kirsch's (1898) elasticity solution and a linear Mohr–Coulomb failure criterion. In another more elaborate type of model (Zheng et al., 1988) the stresses around the borehole were compared to those required to cause failure according to a spalling criterion for the immediate zone around the borehole wall and the Mohr–Coulomb criterion for the remaining rock.

Thus, underground excavations in rock in the form of deep boreholes and tunnels or caverns display usually some degree of deviation from the circular shape either due to optimization of their shape or due to sidewall failure of the rock mass. Almost all relevant modeling work has been based on Kirsch's solution for elastic stresses around circular holes. Since a circular solution cannot describe an actual notched-hole geometry it is evident that a completely new solution is necessary. As it is noted by Cheatham (1993) an exact elasticity solution for a breakout configuration that is quite similar to the initial circular cavity breakout shape (Fig. 2) has been published by Mitchell (1966). By using the method of complex potential funtions $\phi(z)$, $\psi(z)$ of Muskhelishvili (1963), Mitchell (1966) has solved the stress-concentration-problem for a doubly symmetrical hole whose boundary consists of three intersecting circles. However, it would appear that the evaluation of the full-field stress distribution around the hole, and consequently the stress-gradient effect, has not been pursued by the author since he did not present the solution for the second potential function $\psi(z)$ of the complex variable $z = x + \mathrm{i}y$. Therefore, at this point it should be made clear that Mitchell has not presented the complete solution for the elastic stresses and displacements [1] around the doubly symmetric hole. Further, the same investigator did not consider the effect of internal pressure. However, one may argue that the exercise of finding the complete representation of the stresses and displacements around notched openings analytically is still warranted in view of availability of many accurate and easy to use finite element, finite difference, or boundary element computer codes. In order to reply to this argument, we simply refer here to the statement made by Carranza-Torres and Fairhurst (1999):

> ...Although the complex geometries of many geotechnical design problems dictate the use of numerical modeling to provide more realistic results than those from classical analytical solutions, the insight into the general nature of the solution (influence of the variables involved, etc.) that can be gained from the classical solution is an important attribute that should not be overlooked. Some degree of simplification is always needed in formulating a design analysis and it is essential that the design engineer be able to assess the general correctness of a numerical analysis wherever possible. The closed-form results provide a valuable means of making this assessment...

Based on the above considerations, a semi-analytical solution of the notched circular cylindrical opening in elastic, isotropic and homogeneous rock is presented in Section 3, that is based on the powerful conformal mapping method [2] in conjunction with a numerical scheme (Section 2) and closed-form complex function solutions. Subsequently in Section 4, Mitchell's stress-concentration-solution for the doubly symmetric hole is compared successfully with the proposed solution. Moreover, stress and displacement analysis results of the present solution are compared with those predicted by the FLAC^{2D} finite differences code. In the same section, it is also illustrated that this solution may be applied to solve non-rounded diametrically opposed notches, such as the dog-eared (wedge-shaped) notches. In Section 5, the effect of

[1] The displacement solution is of interest to the geotechnical engineer for the design of tunnel or borehole support and for the back-analysis of tunnel or borehole closure measurements.

[2] Jaeger and Cook (1976) in their celebrated book of Rock Mechanics state explicitly that "... By far the most powerful method for the solution of two-dimensional problems is the detailed use of complex variable theory and conformal representation as developed in the books of Muskhelishvili (1963) and Savin (1961)..."

internal pressure on borehole stability is demonstrated. Also, a theoretical background is developed, based on the stress-gradient effect due to stress concentrations caused by extremely curved surfaces, that may lead to a better understanding of the stability of cavities in rock. The capability of this theory to capture the stability of breakout formation is also demonstrated in this section. Finally, Section 6 presents the main conclusions of this work.

2. The conformal mapping representation of notched openings

The methodology starts with the conformal mapping [3] of the boundary of the notched hole C and its exterior region S (Fig. 3a) into the interior of the circle with unit radius (region Σ in Fig. 3b). The position of every point in the physical z-plane with $z = x + \mathrm{i}y = r\mathrm{e}^{\mathrm{i}\alpha}$ is mapped into the unit circle in the ζ-plane with $\zeta = \xi + \mathrm{i}\eta = \rho\mathrm{e}^{\mathrm{i}\theta}$ by the complex function

$$z = x + \mathrm{i}y = \omega(\zeta) = \frac{\alpha_0}{\zeta} + \sum_{k=1}^{n} \alpha_{2k-1}\zeta^{2k-1}, \quad |\zeta| \leqslant 1 \tag{1}$$

where the constant coefficients α_0, α_{2k-1} $(k = 1, 2, \ldots, n)$ are real numbers since the loading and geometry configuration of the problem exhibits symmetry with respect to both Ox- and Oy-axes. These coefficients must be chosen in such a manner that the curve is an adequate approximation to that of Fig. 3a. Note that the point z describes the contour C in the z-plane in an anti-clockwise direction, as the point ζ moves around the circle in the ζ-plane, likewise in a clockwise direction (Fig. 3b). This is because the opening exterior infinite region is mapped into an interior finite region. Also, the boundary of the notched hole C is mapped onto the circumference γ of the unit circle (with $\zeta = \mathrm{e}^{\mathrm{i}\theta}$ along γ).

The parametric representation of the curves in the Oxy-plane transformed by (1) has as follows:

$$\begin{aligned} x &= \frac{\alpha_0 \cos\theta}{\rho} + \sum_{k=1}^{n} \rho^{2k-1}\alpha_{2k-1}\cos(2k-1)\theta \\ y &= -\frac{\alpha_0 \sin\theta}{\rho} + \sum_{k=1}^{n} \rho^{2k-1}\alpha_{2k-1}\sin(2k-1)\theta \end{aligned} \tag{2}$$

The transformation of the Cartesian coordinates (x, y) through the parametric equations (2) will result in a new orthogonal system of curvilinear coordinates (Fig. 4a) that corresponds to the families of curves $\rho =$ constant (ct) and $\theta =$ constant (ct) in the ζ-plane (Fig. 4b). The parametric representation of the notched opening boundary C is obtained by setting $\rho = 1$ into relationships (2).

The algorithm for the computation of the constant coefficients α_0, α_{2k-1} $(k = 1, 2, \ldots, n)$ that has developed in this work has as follows:

(i) First, the curve C of the boundary of the opening is digitized by means of a suitable CAD software. Then it is divided into $(m + 1)$ sampling points $(m \geqslant 1)$, with the first and the last points coinciding, in an anti-clockwise sense as it is shown in Fig. 5. The density of these points is increased in regions of large variations of the radius of curvature (i.e. in these points of the boundary in which a large deviation of the tangent to the boundary and the normal line to the radius connecting the point with the centre of coordinates occurs). In a first approximation, it is assumed that these points correspond to $\theta = 2\pi/m$ equidistant points along the boundary of the unit disk in a clockwise sense.

[3] A transformation of the form $x = x(\xi, \eta)$, $y = y(\xi, \eta)$ is said to be conformal if the angle between intersecting curves in the (ξ, η)-plane remains the same for corresponding mapped curves in the (x, y)-plane.

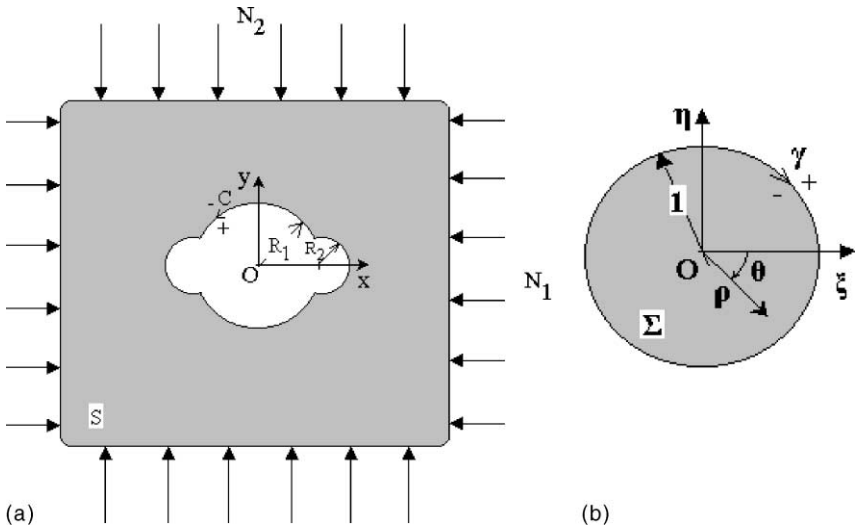

Fig. 3. (a) Doubly symmetric hole subjected to an anisotropic stress field and system of coordinates and (b) disk of unit radius and system of coordinates.

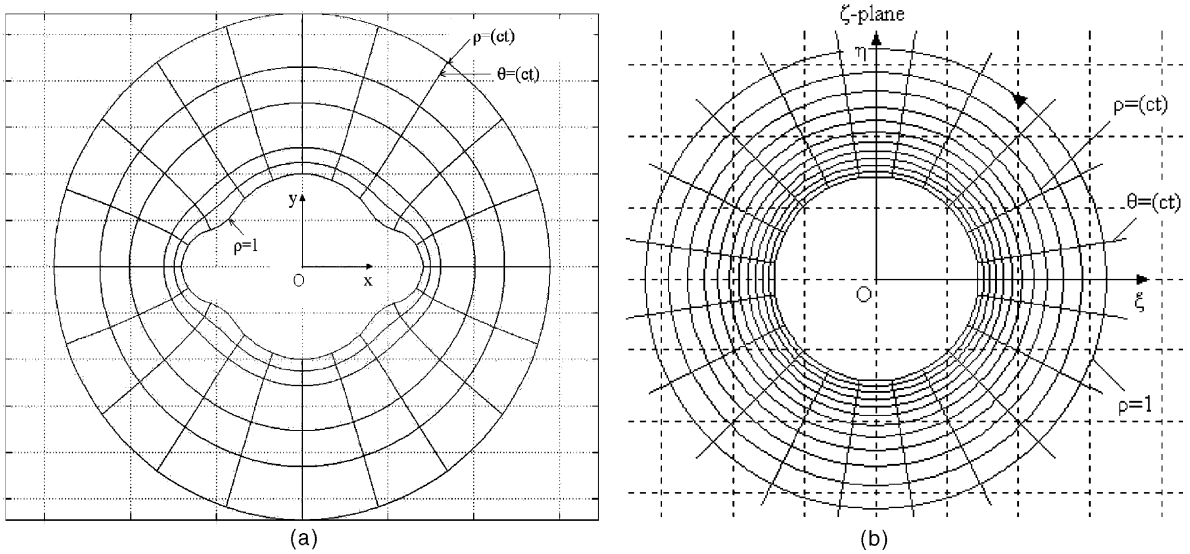

Fig. 4. Conformal mapping of (a) an infinite soil/rock mass surrounding a notched hole into (b) the interior of the unit circle $\rho \leqslant 1$.

(ii) Next, we calculate, in a first approximation, the constant coefficients of the mapping function (1) by solving the overdetermined linear system of m equations with n unknowns with an appropriate least squares numerical scheme

$$AX = B \Longleftrightarrow X = (A^{\mathrm{T}}A)^{-1}A^{\mathrm{T}}B \tag{3}$$

in which m is the number of sampling points and the matrices are defined as follows:

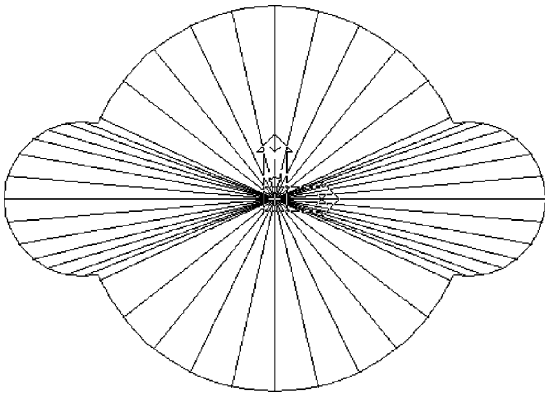

Fig. 5. Example of distribution of sampling z-points for the hole with $R_2/R_1 = 0.4$.

$$A = \begin{bmatrix} \frac{1}{\zeta_0} & \zeta_0 & \zeta_0^3 & \cdots & \zeta_0^{2n-1} \\ \frac{1}{\zeta_1} & \zeta_1 & \zeta_1^3 & \cdots & \zeta_1^{2n-1} \\ \frac{1}{\zeta_2} & \zeta_2 & \zeta_2^3 & \cdots & \zeta_2^{2n-1} \\ \vdots & \vdots & \vdots & \vdots & \vdots \\ \frac{1}{\zeta_m} & \zeta_m & \zeta_m^3 & \cdots & \zeta_m^{2n-1} \end{bmatrix}, \quad X = \begin{bmatrix} \alpha_0 \\ \alpha_1 \\ \alpha_3 \\ \vdots \\ \alpha_{2n-1} \end{bmatrix}, \quad B = \begin{bmatrix} z_0 \\ z_1 \\ z_2 \\ \vdots \\ z_m \end{bmatrix} \tag{4}$$

(iii) After the first estimation of the constant coefficients α_0, α_{2k-1} $(k = 1, 2, \ldots, n)$ the new points on the physical boundary of the opening at the z-plane are calculated by virtue of the mapping function (1). Subsequently, for each point predicted by the mapping function, the intersection of the line that connects this point and the centre of coordinates with the prescribed physical boundary is used as the new z-value. These new z-values are next substituted into the system (4) which is solved for the estimation of the new improved values of α_0, α_{2k-1} $(k = 1, 2, \ldots, n)$.

(iv) This iterative procedure is continued until a prescribed small error is achieved, that is equal to the sum of the squares of the differences between the actual and predicted boundary points of the hole.

Fig. 6a and b illustrates the approximations of the boundary of the hole by using the above algorithm when $R_2/R_1 = 0.1$ and $R_2/R_1 = 0.4$, respectively. It was found that $n = 14$ is adequate for the good approximation of the curves of holes in the range of relative radii $R_2/R_1 = 0.1 - 1$.

3. Solution of the traction boundary value problem of the notched hole

In the frame of the theory of complex potential functions, the boundary condition for the case that forces are prescribed along the contour γ of the unit disk takes the form (Muskhelishvili, 1963)

$$\phi_0(\zeta) + \frac{1}{2\pi i}\int_\gamma \frac{\omega(\sigma)}{\overline{\omega'(\sigma)}}\frac{\overline{\phi_0'(\sigma)}d\sigma}{\sigma - \zeta} = \frac{1}{2\pi i}\int_\gamma \frac{f_0 d\sigma}{\sigma - \zeta} \tag{5}$$

in which $\sigma = e^{i\theta}$ denotes an arbitrary point of the contour γ, and

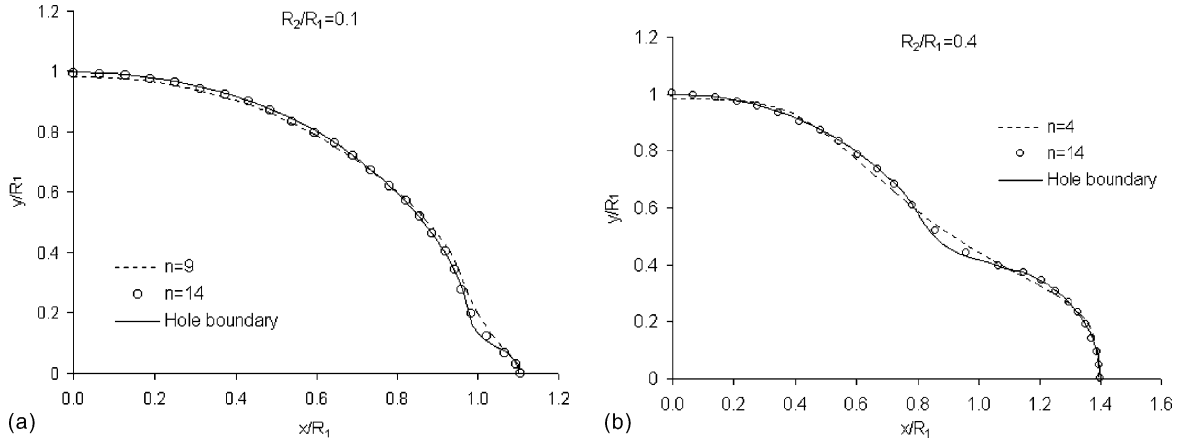

Fig. 6. Approximations of the boundary of the doubly symmetric holes with: (a) $R_2/R_1 = 0.1$ and (b) $R_2/R_1 = 0.4$.

$$f_0(\sigma) = f(\sigma) - \frac{\Gamma\alpha_0}{\sigma} + \frac{\omega(\sigma)}{\overline{\omega'(\sigma)}}\Gamma\bar{\alpha}_0\sigma^2 - \overline{\Gamma'}\bar{\alpha}_0\sigma \tag{6}$$

Also,

$$\Gamma = \frac{1}{4}(N_1 + N_2), \quad \Gamma' = -\frac{1}{2}(N_1 - N_2) \tag{7}$$

with N_1, N_2 referring to the principal stresses at infinity acting along Ox- and Oy-axes, respectively (e.g. Fig. 3a). The quantity $f(\sigma)$ in the case of uniform pressure $-P$, where P is a positive quantity (unless stated otherwise tensile stresses are considered positive quantities) applied to the edge of the hole is given by the relation

$$f(z) = -Pz = -P\omega(\zeta) \tag{8}$$

The methodology of solving the Cauchy integral equation (5) by employing a Laurent series expansion of $\phi_0(\zeta)$ has been presented elegantly by Muskhelishvili (1963). The same author has presented the solution for the elliptical opening, whereas Savin (1961) and Novozhilov (1961) have solved the problems of square and rectangular openings. On the other hand, as it was mentioned in Section 1, Mitchell (1966) was the first investigator who solved the stress-concentration problem of the doubly symmetric hole by employing Muskhelishvili's method. Also, recently, the same methodology has been applied for the solution of tunnels with one axis of symmetry (Exadaktylos and Stavropoulou, 2002).

Proceeding formally, from Eq. (1) it may be inferred that we may write

$$\frac{\omega(\sigma)}{\overline{\omega'(\sigma)}} = b_{2n-3}\sigma^{2n-3} + b_{2n-5}\sigma^{2n-5} + \cdots + b_1\sigma^1 + \frac{b_{-1}}{\sigma} + \mathrm{O}\left(\frac{1}{\sigma^3}\right) \tag{9}$$

wherein the constant coefficients b_{2k-1} $(k = 0, \ldots, n-1)$ are represented in closed-form in terms of the constant conformal mapping coefficients α_0, α_{2k-1} $(k = 1, \ldots, n)$ and $\mathrm{O}(\cdot)$ denotes Landau's order-of-magnitude symbol. Note that we do not present here the closed-form expressions for the b-coefficients for the case $n = 14$ that is used in this work hereafter, since they are lengthy. However, in Appendix A we illustrate the closed-form expressions for $n = 3$. Due to the symmetry of the problem we may write the following polynomial expression of the analytic function $\phi_0(\zeta)$

$$\phi_0(\zeta) = \sum_{k=1}^{n} c_{2k-1}\zeta^{2k-1} \tag{10}$$

where c_{2k-1} $(k = 0, \ldots, n)$ are unknown constant real coefficients to be determined from the boundary conditions. Also the combination of relationships (9) and (10) gives the following relation

$$\frac{\omega(\sigma)}{\overline{\omega'(\sigma)}}\overline{\phi_0'(\sigma)} = \sum_{k=1}^{n-1} K_{2k-1}\sigma^{2k-1} + \mathrm{O}\left(\frac{1}{\sigma}\right) \tag{11}$$

in which the constant real coefficients K_{2k-1} $(k = 1, \ldots, n-1)$ are represented in closed-form in terms of the constant conformal mapping coefficients α_0, $\alpha_{2k-1}(k = 1, \ldots, n)$ and the still unknown constant series terms of the potential function $\phi_0(\zeta)$, i.e. c_{2k-1} $(k = 1, \ldots, n)$ (see Appendix A for the closed-form expressions for K-coefficients for the particular case $n = 3$).

By substituting into (5), the expressions (6), (10) and (11) and evaluating analytically the Cauchy integrals we obtain

$$\sum_{\kappa=1}^{n} c_{2k-1}\zeta^{2k-1} + \sum_{k=1}^{n-1} K_{2k-1}\zeta^{2k-1} = -P\sum_{k=1}^{n} a_{2k-1}\zeta^{2k-1} - \Gamma' a_0\zeta + \Gamma a_0\zeta^2\sum_{k=0}^{n-1} b_{2k-1}\zeta^{2k-1} \tag{12}$$

Next, by comparing the same powers of the complex variable ζ in Eq. (12), the following linear system of complex algebraic equations is obtained for the computation of the constant coefficients $c_1, c_3, \ldots, c_{2n-1}$

$$\begin{bmatrix} 1+K_1(\zeta) & K_1(\zeta^3) & \cdots & K_1(\zeta^{2n-3}) & 0 \\ K_3(\zeta) & 1+K_3(\zeta^3) & \cdots & 0 & 0 \\ K_5(\zeta) & K_5(\zeta^3) & \cdots & 0 & 0 \\ \vdots & \vdots & \vdots & \vdots & \vdots \\ 0 & 0 & 0 & \cdots & 1 \end{bmatrix} \begin{bmatrix} c_1 \\ c_3 \\ \vdots \\ c_{2n-1} \end{bmatrix} = \begin{bmatrix} -Pa_1 - \Gamma' a_0 + \Gamma a_0 b_{-1} \\ -Pa_3 + \Gamma a_0 b_1 \\ \vdots \\ -Pa_{2n-1} + \Gamma a_0 b_{2n-3} \end{bmatrix} \tag{13}$$

where the terms $K_a(\zeta^b)$ denote that part of the constant coefficients K_{2k-1} that contains c_b and is multiplied by the ath power of ζ (as an example, we refer here to the closed-form results that are displayed in Appendix A for $n = 3$). The solution of the linear system of algebraic equations (12) for the unknowns c_{2k-1} $(k = 1, \ldots, n)$ gives the first complex potential as follows:

$$\phi(\zeta) = \frac{\Gamma a_0}{\zeta} + \phi_0(\zeta) \tag{14}$$

Finally, the second complex potential function is given by the formula

$$\psi(\zeta) = \frac{\Gamma'\alpha_0}{\zeta} - \alpha_0(\Gamma + P)\zeta - \left[\frac{\overline{\omega(\zeta)}}{\omega'(\zeta)}\phi_0'(\zeta) - \sum_{k=1}^{n-1} K_{2k-1}\zeta^{2k-1}\right] + \Gamma\alpha_0\left[\frac{\overline{\omega(\zeta)}}{\omega'(\zeta)} - \sum_{k=0}^{n-1} b_{2k-1}\zeta^{-2k-1}\right]\frac{1}{\zeta^2} \tag{15}$$

Then, in polar coordinates (ρ, θ) the radial, tangential and shear stresses denoted as σ_ρ, σ_θ, $\tau_{\rho\theta}$, respectively, and the radial and tangential incremental displacements υ_ρ, υ_θ due to stress relief at the breakout boundary, may be computed by virtue of the following formulae

$$\left.\begin{aligned} &\sigma_\rho + \sigma_\theta = 4\mathrm{Re}\left[\tfrac{\phi'(\zeta)}{\omega'(\zeta)}\right] \\ &\sigma_\rho - \mathrm{i}\tau_{\rho\theta} = 2\mathrm{Re}\left[\tfrac{\phi'(\zeta)}{\omega'(\zeta)}\right] - \tfrac{\zeta^2}{\rho^2\bar{\omega}'(\bar{\zeta})}\left[\bar{\omega}(\bar{\zeta})\{\phi'(\zeta)/\omega'(\zeta)\}' + \omega'(\zeta)\psi'(\zeta)\right] \\ &2G(\upsilon_\rho + \mathrm{i}\upsilon_\theta) = \tfrac{\bar{\zeta}}{\rho}\tfrac{\bar{\omega}'(\bar{\zeta})}{\rho|\omega'(\zeta)|}\left[\kappa\phi_0(\zeta) - \tfrac{\omega(\zeta)\bar{\phi}_0'(\bar{\zeta})}{\bar{\omega}'(\bar{\zeta})} - \bar{\psi}_0(\bar{\zeta})\right] \end{aligned}\right\} \tag{16}$$

where primes denote differentiation (i.e. $\phi' \equiv d\phi/d\zeta$), $|\cdot|$ denotes the absolute value or the modulus of the complex quantity it encloses, κ denotes Muskhelishvili's constant with $\kappa = 3 - 4\nu$ for plane strain conditions, $G = E/2(1+\nu)$ is the shear modulus, and E, ν is the Young's modulus and Poisson's ratio of the isotropic rock/soil mass, respectively. Also, the displacements referred to the Cartesian coordinate system Oxy are given by

$$2G(u_x + iu_y) = \kappa\phi_0(\zeta) - \frac{\omega(\zeta)\bar{\phi}_0'(\bar{\zeta})}{\bar{\omega}'(\bar{\zeta})} - \bar{\psi}_0(\bar{\zeta}) \tag{17a}$$

in which we have put

$$\psi_0(\zeta) = \psi(\zeta) - \Gamma'\omega(\zeta) \tag{17b}$$

The above expression for the displacements (17a) corresponds to the case of excavating a hole in a pre-stressed medium in which the surface tractions are totally relieved along the contour of the hole. That is, the displacements fade-out with distance from the hole. The same holds true for the stress expressions (16), since the considered boundary value problem of the hole in an initially unstressed medium yields—by means of the superposition principle—the same stress distribution with the problem of the hole excavated in a pre-stressed medium.

4. Comparison of the closed-form solution for the doubly symmetric hole with existing analytical stress-concentration solutions and the FLAC finite differences code

In order to compare the present solution with the Mitchell's (1966) solution pertaining to the stress-concentration factor (SCF) at the notch, we consider the doubly symmetric hole that is subjected to far-field uniaxial compression N_2. Graphical results pertaining to the variation of the SCF, $K_t = \sigma_\theta(\theta = 0°)/N_2$, with the radii ratio R_2/R_1, are presented in Fig. 7. As it was noted by Mitchell, for very small values of the notch radius, i.e. $R_2 \to 0$, the local stress distribution will be the same as that around a semi-circular notch in a half-space. Since the SCF of a circular hole is equal to 3 and that of a semi-circular notch in a half-space is 3.08, the limiting value of K_t as R_2 tends to zero is $3 \times 3.08 = 9.24$. On the other hand, as $R_2 \to \infty$ the SCF tends to the value of 3.

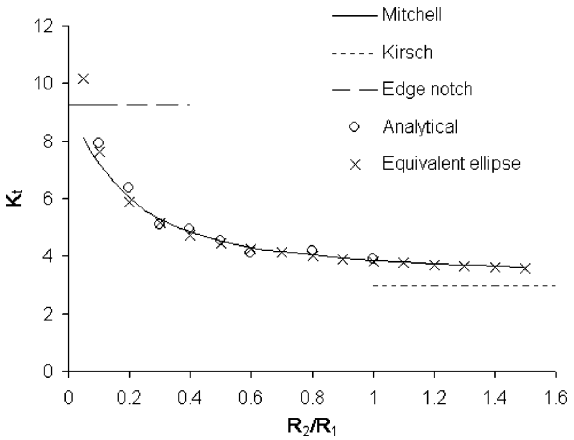

Fig. 7. Comparison of the predicted variation of the stress concentration factor K_t with the ratio of radii of the notch and the hole for uniaxial compression at infinity with Mitchell's and 'equivalent ellipse' solutions.

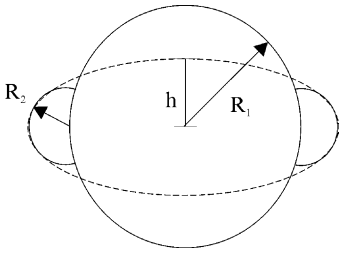

Fig. 8. Equivalent ellipse concept.

Mitchell (1966) have demonstrated that his results can be approximated with a high degree of accuracy by an 'equivalent ellipse' (Fig. 8). The length of the horizontal semi-axis of the equivalent ellipse, herein denoted by the symbol b, is equal to the that of the doubly symmetric hole, i.e.

$$b = R_1 + R_2 \tag{18}$$

whereas the length of the vertical semi-axis is found by requiring that the radius of curvature of the ellipse at the end of the horizontal semi-axis to be equal to the radius of the notch. Since the radius of curvature of the ellipse at the end of the horizontal axis is given by

$$R_{\mathrm{H}} = \frac{h^2}{R_1 + R_2} \tag{19}$$

where R_{H} is the horizontal radius of curvature at wall, and h denotes the semi-height of the elliptical opening, then by putting $R_{\mathrm{H}} = R_2$ one finds

$$h = \sqrt{R_2(R_1 + R_2)} \tag{20}$$

The fundamental solution in terms of the complex potentials ϕ, ψ for the elliptic hole with tractionless edge subjected to far-field uniaxial compression N_2 is given by Muskhelishvili (1963). The recovered result from Muskhelishvili's fundamental solution concerning the distribution of the hoop stress along the periphery of the cavity reads as follows:

$$\sigma_\theta(\rho = 1, \theta) = \frac{(b-h)^2 + (b+h)^2 \cos 2\theta}{b^2 + h^2 - (b^2 - h^2)\cos 2\theta} N_2 \tag{21}$$

The elastic SCFs at the tips of the ellipse is obtained from the above expression (21), i.e.

$$K_t^{\mathrm{e}} = \frac{\sigma_\theta(1, 0^\circ)}{N_2} = \left(\frac{2b}{h} + 1\right) \tag{22}$$

As it is displayed in Fig. 7 the equivalent ellipse solution displays excellent agreement with Mitchell's solution. Finally, the derived closed-form solution agrees very well with both models with the maximum relative error with regard to Mitchell's solution not exceeding 5% in the range of relative radii $0.1 \leqslant R_2/R_1 \leqslant 1$.

Next, in order to demonstrate the potential applications of the proposed solution in soil/rock engineering we investigate the case of the notched hole with traction-free boundary subjected to all-around uniform compression $N_1 = N_2 = N$ at infinity. Since Mitchell has not pursued this problem, the results of the present closed-form solution are compared to those referred to the equivalent elliptic hole and to the results of FLAC^{2D} finite difference numerical model (ITASCA, 1995). [4]

[4] This numerical model is used extensively worldwide for the design of underground excavations in geomaterials.

Later we will see that we also need the SCF-solution of the equivalent ellipse. The recovered result from Muskhelishvili's fundamental solution concerning the distribution of the hoop stress in the direction of the major axis of the elliptical hole, $\theta = 0^\circ$ (by adopting the same polar coordinate system as in the case of the doubly symmetric hole, e.g. Fig. 3), as well as along the periphery of the cavity, respectively, read as follows:

$$\sigma_\theta(\rho = 1, \theta) = \frac{4bhN}{b^2 + h^2 - (b^2 - h^2)\cos 2\theta} \tag{23}$$

The elastic SCFs at the tips of the ellipse is obtained from (23) as follows:

$$K_t^{\mathrm{e}} = \frac{\sigma_\theta(1, 0^\circ)}{N} = \frac{2b}{h} \tag{24}$$

An example of FLAC zone geometry employed in this study is illustrated in Fig. 9. It may be observed the zone size is increasing away from the hole boundary. The symmetry of the problem with respect to *Ox*- and *Oy*-axes has been exploited in the numerical model by considering only the upper-right quarter part. Roller boundaries are employed to model zero displacement along the respective lines of symmetry.

The dependence of the SCF on the ratio R_2/R_1 is presented graphically in Fig. 10. In the same figure, the limiting value of the SCF as $R_2 \to \infty$, that corresponds to the circular hole, SCF = 2, has been also plotted with a dashed line. Also it may be seen that the predictions of the FLAC^{2D} model are in reasonable agreement with the closed-form and equivalent ellipse solutions apart for $R_2/R_1 < 0.2$. This is due to the fact that the grid size should be appreciably smaller than the notch size in order for the finite differences model to be accurate. On the contrary, the analytical solution is not subjected to such a constraint.

The distributions of the dimensionless hoop stress around the doubly symmetric hole for the particular case of a breakout with $R_2/R_1 = 0.4$ that is subjected to all-around uniform pressure of 1 MPa at infinity, are illustrated in Fig. 11a. Note that in this section compressive stresses are considered to be positive quantities. Also, Fig. 11b illustrates the contour plot of tangential stresses around the hole that is predicted by the closed-form solution. The two predictions compare very well, apart from the region surrounding the corner point depicted by the intersection of the two circles. The reason for this discrepancy is: (i) because the conformal mapping function introduces some smoothing of the corner region as it is displayed in Fig. 6b, and (ii) as it is illustrated in Fig. 12a, the numerical FLAC model predicts finite radial and shear stresses at the notch region whereas the closed-form solution predicts almost zero tractions along the boundary of the hole (Fig. 12b).

The variations of the tangential and radial stresses along the *Ox*-axis of the doubly symmetric hole are also of interest due to the existence of the stress-gradient effect, which in turn influences the strength of opening wall (Jaeger and Cook, 1976). Fig. 13 illustrates the distributions of the tangential and radial stresses along *Ox*-axis predicted by the FLAC^{2D} finite differences scheme and by the proposed solution. It may be seen from these figures that σ_θ drops from its maximum and approaches the value of 1 MPa at large radii r. Furthermore, the example of Fig. 13 reflects the general result, namely major perturbations to the applied stress field occur only within approximately a dimensionless distance $(1 + R_2/R_1)$ from the boundary of the hole, with the greatest stress gradients confined to a highly localized region of dimension just about R_2/R_1 surrounding the position of maximum concentration. Some discrepancy of the numerical solution from the analytical solution close to the notch tip is due to the error introduced by the numerical model at this region. That is, the numerical model predicts finite shear and radial stresses at the notch tip ($\theta = 0^\circ$ in Fig. 12a).

Fig. 14a presents the comparison between FLAC and analytical models pertaining to the variation of horizontal and vertical displacements, u_x, u_y, around the plane strain notched hole characterized by $E = 6.77$ GPa and $\nu = 0.21$. From this figure, it may be seen that both predictions are in very good agreement. The analytical solution is also illustrated by the displacement plot in Fig. 14b.

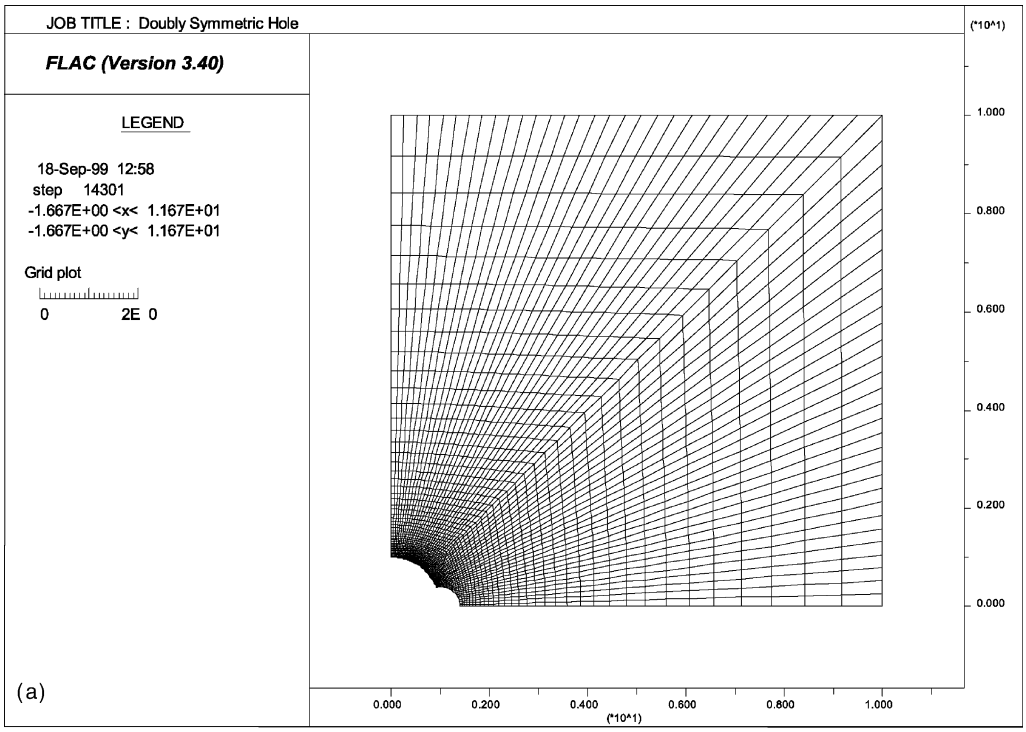

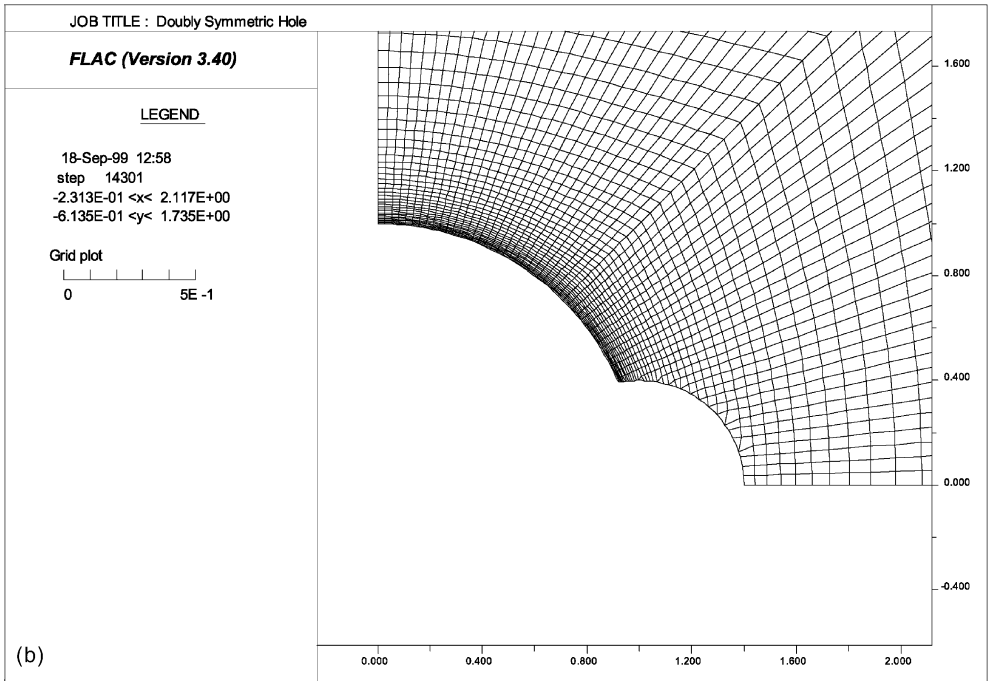

Fig. 9. (a) FLAC finite difference grid for the case of breakout with $R_2/R_1 = 0.4$ and (b) detail of the zone geometry near the boundary of the notched hole.

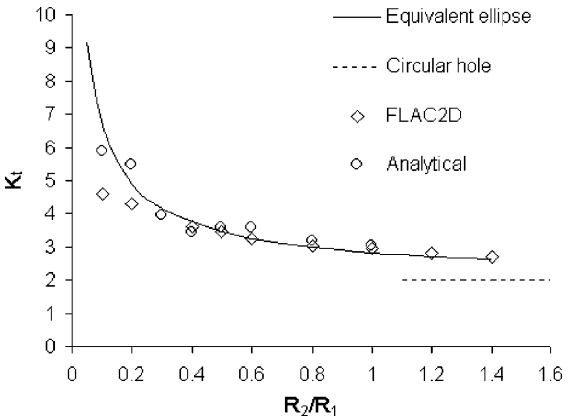

Fig. 10. Comparison of the SCF for the equivalent ellipse subjected to far-field uniform compression with the results of analytical solution and FLAC numerical solution.

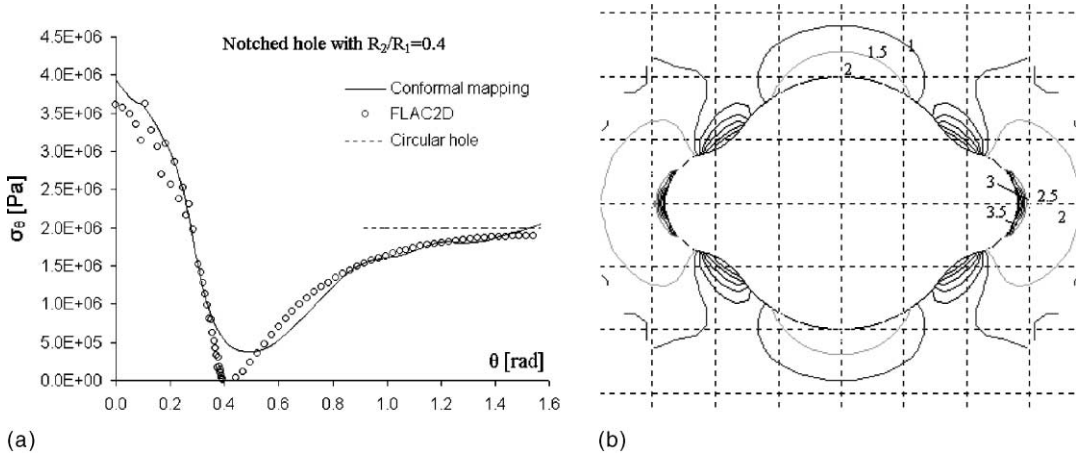

Fig. 11. (a) Comparison of the hoop stress, σ_θ, along the periphery of the doubly symmetric hole, and the circular hole and (b) contours of hoop stress, σ_θ (in MPa), predicted by the analytical solution.

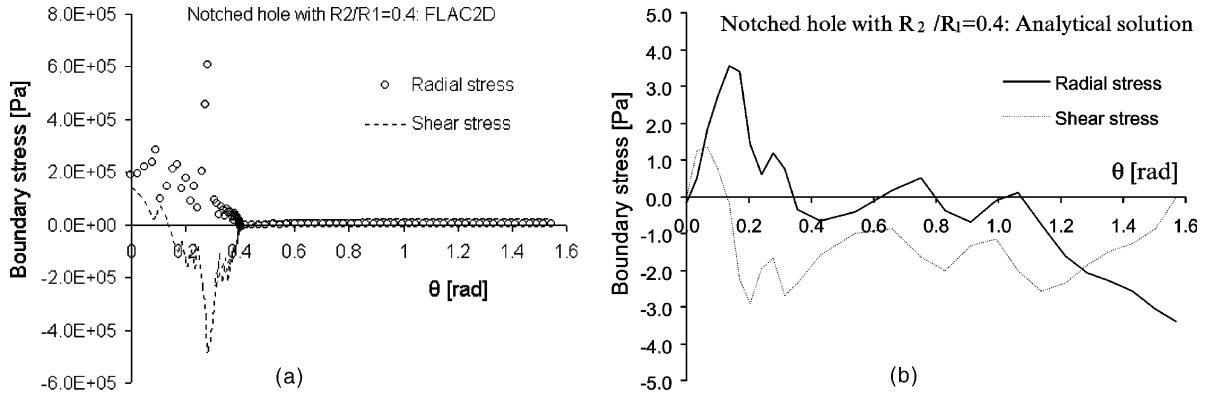

Fig. 12. Plot of radial and shear stresses around the boundary of the opening: (a) prediction of the FLAC numerical model and (b) prediction of the conformal mapping solution.

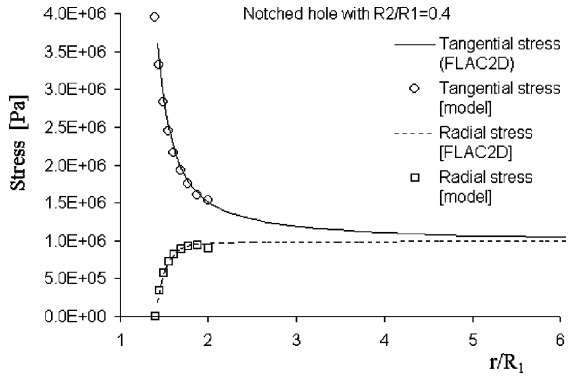

Fig. 13. Distribution of the normalized hoop stress σ_θ and radial stress σ_r, along Ox-axis for the doubly symmetric hole characterized by $R_2/R_1 = 0.4$ and subjected to all-around uniform pressure of 1 MPa. Note that concentration is localized within $(R_1 + R_2)$ from tip, with high stress gradients within approximately R_2 from tip.

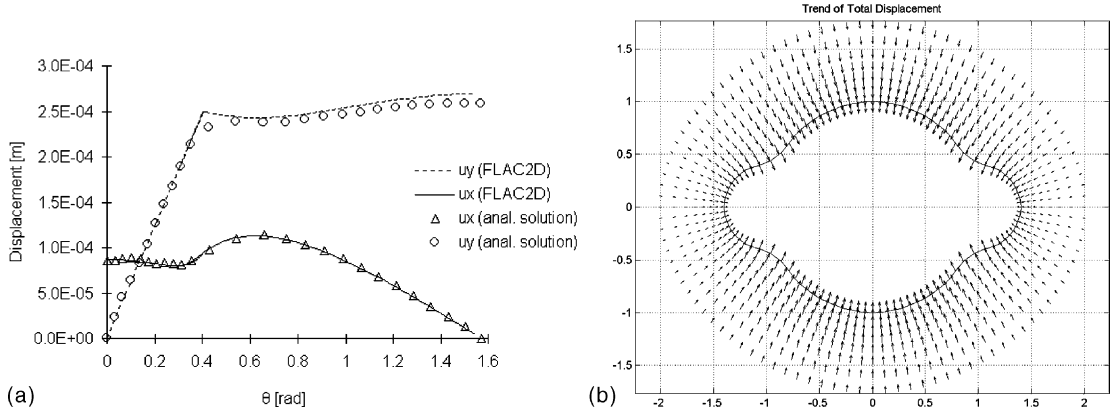

Fig. 14. (a) Plot of the vertical and horizontal displacements along the periphery of the doubly symmetric hole characterized by $R_2/R_1 = 0.4$ predicted by the numerical and analytical model and (b) displacement vectors predicted by the analytical model.

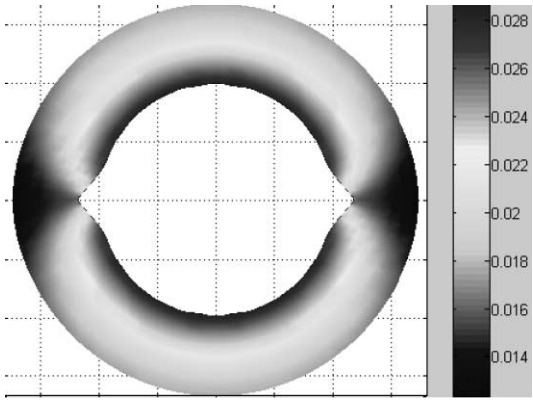

Fig. 15. Hole with dog-ear cross-sectional shape. The angle subtended at the centre of the hole by the intersection of the breakout and the circumference of the opening is equal to 30° and the length of the notch from the circumference is $0.2 \times R_1$ ($R_1 = 1$). Colormap of the distribution of radial displacement for $N_1/E = N_2/E = -1/50$ and $\nu = 0.3$.

It is noted here that the semi-analytical solution holds true for any shape of anti-diametrical notches at the boundary of the hole. As an example, we present here in Fig. 15 displacement data for the particular case of dog-eared notched hole configuration.

5. Stability of borehole breakouts

5.1. Effect of internal pressure on borehole collapse

One of the borehole stability controlling parameters is the borehole pressure, as it influences the stress-concentration effect directly. In this paragraph we investigate the stress-concentration effect in circular and notched-circular holes by employing the semi-analytical solution presented in Section 3. When the absolute pressure P that is exerted on the boundary of a borehole drops, the tangential stress at the wall increases, and it results in a borehole collapse if this stress exceeds the biaxial compressive strength of the rock.

For the case of the circular–cylindrical hole subjected to a biaxial far-field principal stresses and internal pressure, the variation of the tangential stress around its boundary is given by the formula [5] (Muskhelishvili, 1963)

$$\frac{\sigma_\theta}{\sigma_y} = 1 + k + 2(1-k)\cos 2\theta + \frac{P}{\sigma_y} \tag{25}$$

wherein $k = \sigma_x/\sigma_y$. The distribution of the tangential stress around the circular hole is illustrated in Fig. 16 for various internal pressures for the case of $k = 0.9$.

On the other hand, the variation of tangential stress around the notched hole with $R_2/R_1 = 0.4$ is shown in Fig. 17, for various borehole pressures. For both cases it may be seen that the highest stress concentration occurs always at the points of the contour corresponding to $\theta = 0°$, 180°, i.e. along the direction of the minimum principal stress. Lowering the borehole pressure results in an increase of the tangential stress at these points.

From Fig. 18, it is observed that the following three conditions are possible.

(a) The condition $-P/\sigma_y = 1.2$ in which the maximum tangential stress is the same for the notched and the circular holes.
(b) The condition $-P/\sigma_y > 1.2$ in which the maximum tangential stress is higher for the circular hole than for the notched hole.
(c) The condition $-P/\sigma_y < 1.2$ in which the maximum tangential stress is higher for the notched hole than for the circular hole.

These three conditions can be interpreted as follows. For case (a), there is no preferred cross-sectional hole shape, that is, if the circular hole is stable, it is equally stable in a notched shape. For the case (b), the notched circular hole will lead to a lower tangential stress, hence it is more stable than the circular hole. Finally, for the case (c), a collapsed circular hole will lead to a higher stress concentration. This in turn may lead to an unstable failure process.

From the above discussion, it is clear that the borehole pressure should be equal or higher than 1.2 times the highest normal stress on the borehole to avoid collapse. However, practical well situations it is not always possible to keep the borehole pressure sufficiently high to fully avoid collapse. A lower borehole pressure may initiate a collapse that will stabilize by some mechanism other than classical linear elastic rock

[5] In this section, we consider compressive stresses as negative quantities.

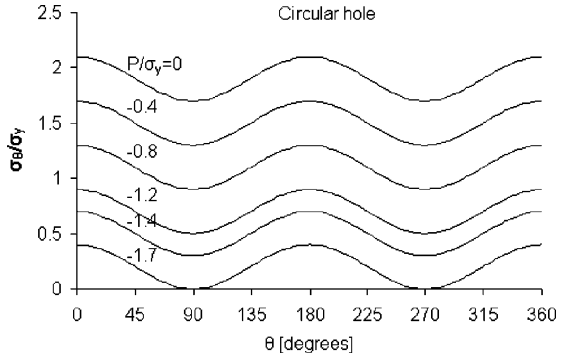

Fig. 16. Distribution of dimensionless tangential stress around the circular hole for various borehole pressures at hand and for $\sigma_x/\sigma_y = 0.9$.

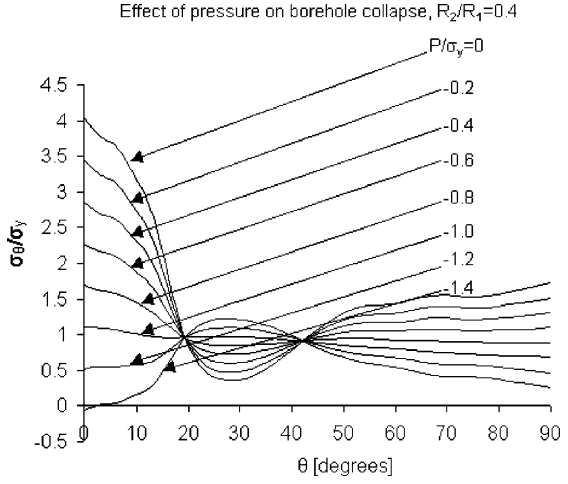

Fig. 17. Distribution of dimensionless tangential stress around the doubly-symmetric hole with $R_2/R_1 = 0.4$ for various borehole pressures at hand and for $\sigma_x/\sigma_y = 0.9$.

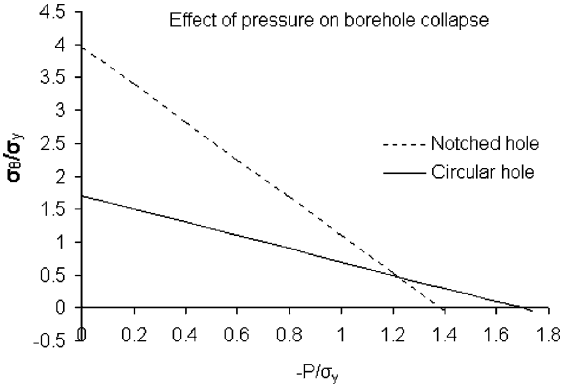

Fig. 18. Maximum dimensionless tangential stress at $\theta = 0°$ as a function of borehole pressure for $\sigma_x/\sigma_y = 0.9$.

behaviour. Hence, there is a need to investigate the stabilizing effect in boreholes. This is performed in the next paragraph.

5.2. The theory of stress-mean-value and the self-support effect

The theories of continuum mechanics (e.g. elasticity and plasticity) use idealized models mostly based on the assumption of a continuous distribution of matter, as opposed to statistical theories of mechanics that are based on the assumption of a discrete distribution of matter. In the framework of local continuum theories, quantities such as stress and strain, represent statistical mean values taken over very small ranges of volume. Consequently continuum theories cannot give satisfying predictions of the behaviour of the material within very small ranges of volume, if high gradients of stress and strain occur. Especially these local theories cannot describe processes with dominating structure effects since all material qualities producing effects of such kind had been eliminated by introducing the idealized models. Within the field of strength of materials the above restriction becomes very important in connection with problems of high stress concentration as caused by extremely curved surfaces, e.g. at holes and notches. In such cases, the classical theory of elasticity predicts high values of stress and strain which are replaced by mean values.

Mathematically speaking, if

$$\bar{f} = f(x) \tag{26}$$

is the value of the function f in the middle of the interval $[x - L/2, x + L/2]$ and

$$\langle f \rangle = \frac{1}{L} \int_{-L/2}^{L/2} f(x + \mathrm{d}x)\, \mathrm{d}x \tag{27}$$

is the mean value of function f in the same interval, then the following relationship holds true

$$\langle f \rangle = \bar{f} - \frac{L^2}{48} \frac{\mathrm{d}^2 f}{\mathrm{d}x^2}\bigg|_x + \mathrm{O}(L^4) \tag{28}$$

The above simple relation (28) means that if the function f is either constant or varies linearly with the variable x in the open interval $[x - L/2, x + L/2]$ then the trapezoidal rule is valid and

$$\langle f \rangle = \bar{f} \tag{29}$$

On the other hand, if f is characterized by intense curvature in the region of interest—i.e. the notch tip region—then the above formula has to be corrected by taking also into account the second term in (28).

By such a simple mathematical procedure an approximate representation of a fundamental structure effect becomes possible which is called here "self-support-effect". It is worth noting that the same stress-mean value approach taken over a finite length normal to the surface within the range of high stress concentration was followed by Neuber (1936) to develop his theory of sharply curved notches. The intrinsic length scale L of structure appearing in (27) and (28) represents an additional material property. In this way, from (27) a 'comparison stress' may be defined that is calculated be means of a suitable strength hypothesis valid for the material. Since practical experience indicates that the spalling occurs in the region of maximum tangential stress around the boundary of the opening then the simple maximum-compressive-stress criterion for brittle materials is the most appropriate and takes the following form

$$\sigma_\theta \geqslant \sigma_0, \quad \theta = 0^\circ \tag{30}$$

where σ_0 is the unconfined compressive strength of the rock. Thus, the comparison stress in this case is the hoop stress along the major axis of the notched hole and the stress-mean-value becomes

$$\langle\sigma\rangle = \frac{1}{L}\int_{r=0}^{L}\sigma_\theta(r)\,\mathrm{d}r \tag{31}$$

where the value of the comparison stress $\sigma_\theta(r)$ may be found from (16) and r denotes the radial distance from the notch tip (i.e. at $\theta = 0°$). In most technical quasi-brittle materials, such as rock, the domains in the vicinity of the highly stress point participate in the force transmission more intensively than according to the linear theory of elasticity, during the endangered point itself is somewhat relieved; this self-support-effect of a notched hole is taken into account by the above formula (31). It should be noted here that the present theory of stress-mean-value is based on the assumption of the continuity of material at the notch tip region. However, rock microcracking in front of the notch may be taken into account by recourse to the famous "surface energy" concept of Griffith and Irwin. Thus, by denoting the surface energy of the rock—reflecting rock microcracking—by the symbol γ and by dividing it by the modulus of elasticity of the rock E we get

$$L = \frac{\alpha\gamma}{E} \tag{32}$$

wherein α is some dimensionless constant that accounts for the density of microcracks that are developed in the process zone in the vicinity of the notch tip. The quantity L has the dimensions of a length, and it may be considered as a characteristic micro-scale length of the rock. Therefore, the effect of microcracks is reflected into the intrinsic length scale L of the rock that is responsible for the stabilization phenomenon of the borehole, as is it will be demonstrated below.

By keeping in mind that the geometry of the breakout plays a key role on the hoop stress distribution near the notch and its stability, we consider here a breakout geometry that resembles closely real-life breakouts as those shown in Fig. 19. Our "elliptical breakout model" is constructed by a circular hole of radius r_i and an intersecting ellipse with the same centre and semi-axes a and b ($a > b$) with $a = r_\mathrm{i} + d$, $b = r_\mathrm{i} - d$ (d = breakout depth) subjected to far-field principal stresses $\sigma_\mathrm{H} \geqslant \sigma_h$ (Fig. 20a). The breakout propagation is simulated with consecutive ellipses characterized by larger semi-axis, a, than the previous one and so on (Fig. 20b). The conformal mappings of successive borehole breakouts are estimated by the proposed numerical algorithm (Fig. 20c).

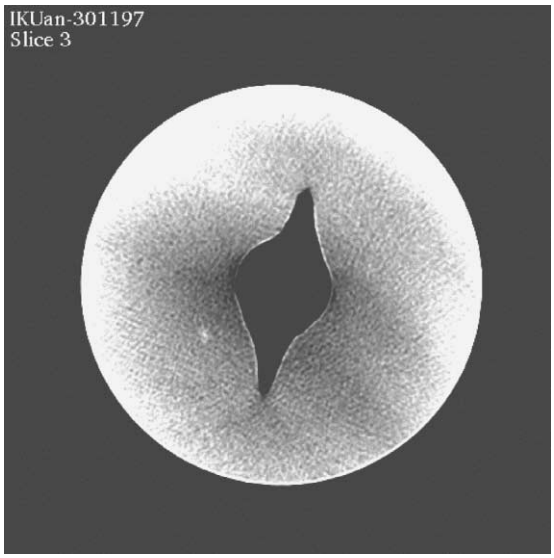

Fig. 19. Borehole breakout configuration in rock (with the courtesy of Papamichos (2002)).

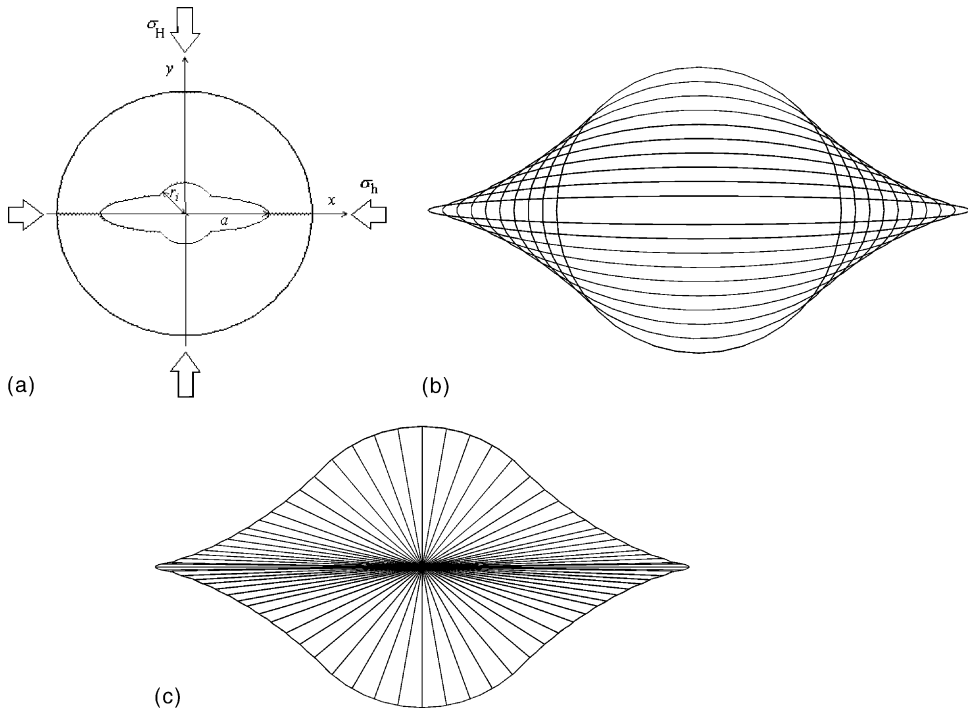

Fig. 20. (a) Geometry and loading configurations for the elliptical breakout; (b) assumed "elliptical" breakout development and (c) method of sampling along the digitized contour of the notched hole for the numerical evaluation of the conformal mapping coefficients.

In Fig. 21, the dependence of the SCF, $K_t = \sigma_\theta/\sigma_h$, on the slenderness, $s = 1 + d/r_i$, for a stress ratio of $k = \sigma_h/\sigma_H = 0.5$ and for various values of the dimensionless length scale $\lambda = L/r_i$, is displayed. From this figure the following points may be noted:

(i) For $\lambda = 0$ and for $s = 1$ which means that the hole is circular, the SCF takes the value of $K_t = 5$ as it is predicted by the classical elasticity theory.
(ii) Below a certain value of λ, the SCF is always lower than the respective value for lower λ, and increases monotonically with the hole slenderness, thus indicating an always unstable borehole breakout propagation.
(iii) However, for $\lambda \geqslant 0.7$, the elliptical breakout model exhibits first an increase with s, then it takes a peak value and finally it decreases with slenderness. This means that for sufficiently large value of the relative internal length scale of the medium the breakout may develop in a stable manner, i.e. additional external energy is needed for further breakout development. This is demonstrated in another example below.

Fig. 22 displays the dependence of the relative minor horizontal stress on the hole slenderness that is needed for breakout propagation according to the failure criterion (30), for the two values of dimensionless length scale at hand and for constant stress ratio $k = 0.5$. As it was expected, classical elasticity theory (i.e. $\lambda = 0$) predicts always a decreasing relative horizontal stress with hole slenderness. On the other hand, the stress-mean-value theory for sufficiently large intrinsic length scale predicts initially unstable breakout propagation that is followed by a stable propagation phase.

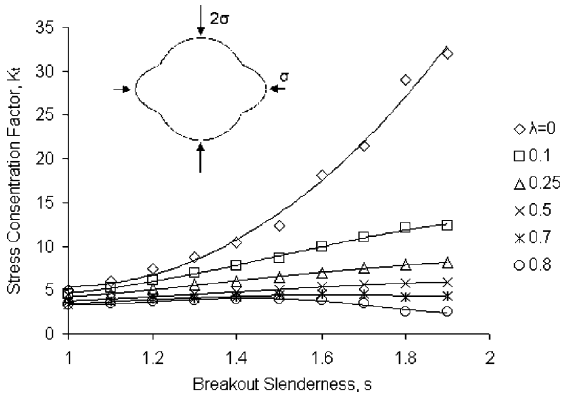

Fig. 21. Plot of the SCF with respect to the slenderness of the hole for various internal length scales and for $k = 0.5$.

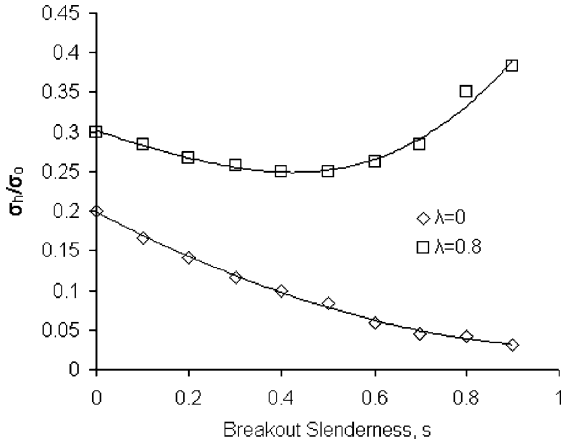

Fig. 22. Plot of the relative minor principal stress with respect to the slenderness of the hole for two values of the internal length scale and for $k = 0.5$.

From the above results, it may be noted that the intrinsic length scale L of a specific rock type with known uniaxial compressive strength may be estimated from laboratory experiments by measuring breakout geometry as well as the final breakout configuration and subsequently calibrating the proposed theory by using L as a control parameter.

6. Conclusions

A semi-analytical solution of the notched hole has been presented that is based on the conformal mapping representation combined with Muskhelishvili complex potentials. The solution can be used for the optimum design of openings in rocks (i.e. boreholes, tunnels, galleries etc.) under given in situ stress field, rock deformability and strength data, or for back-analysis of borehole breakout data for the estimation of in situ stresses. It is a valuable tool for conceptual understanding of how certain parameters—such as notched hole configuration, in situ stresses and internal pressure—affect the stresses and displacements.

The proposed solution can be easily extended to consider either non-symmetrical notched-hole configurations or non-circular cross-sectional shapes of the initial opening by an appropriate choice of the constant conformal mapping coefficients with the CAD/numerical scheme presented in Section 2.

Numerical results have been presented concerning the hole under uniform uniaxial and biaxial far-field compression. It is demonstrated, be means of comparison with an already existing analytical solution and with the FLAC^{2D} finite differences code, respectively, that the analytical solution can be effectively used for studying the stresses and displacements around doubly-symmetrical holes. Of course, it cannot be a substitute for highly versatile and powerful methods of numerical analysis; yet, this solution and likes of it are indispensable when it comes either to testing and calibrating numerical codes or to back-analyze stress, deformation and failure measurements.

Finally, keeping in mind that the continuum theory works well for uniform or linear distribution of quantities such as stress and strain, a stress-mean-value theory is proposed, which is a second-order correction of the classical theory in order to take into account high stress gradient effects in the vicinity of a notch. It is demonstrated that the proposed simple theory in conjunction with a maximum unconfined compression stress criterion is capable to predict the stability of borehole breakouts. This in turn, permits one to use the semi-analytical solution as a very fast solver for in situ back-analyses of televiewer images of borehole breakouts.

Acknowledgements

The authors gratefully acknowledge the comments made by Dr. C. Carranza-Torres as well as the financial support of the European Union Environment Programme 3F—Corinth (Faults, Fractures & Fluids) under contract ENK6-2000-0056.

Appendix A

This example demonstrates that the complex function $\phi(\zeta)$ may be found in closed-form provided that the conformal mapping $\omega(\zeta)$ has been found numerically. In order not to present lengthy expressions for $n = 14$, we consider here a mapping function with three series terms (i.e. $n = 3$) as follows:

$$\omega(\zeta) = \frac{\alpha_0}{\zeta} + \alpha_1\zeta + \alpha_3\zeta^3 + \alpha_5\zeta^5 \tag{A.1}$$

Then Eq. (9) takes the form

$$\frac{\omega(\zeta)}{\omega'(\zeta)} = b_3\zeta^3 + b_1\zeta + \frac{b_{-1}}{\zeta} + \mathrm{O}\left(\frac{1}{\zeta^3}\right) \tag{A.2}$$

wherein

$$\left.\begin{aligned} b_3 &= -\frac{\alpha_5}{\alpha_0} \\ b_1 &= -\frac{\alpha_3 + \frac{\alpha_5\alpha_1}{\alpha_0}}{\alpha_0} \\ b_{-1} &= -\frac{\alpha_1 + \dfrac{3\alpha_5\alpha_3}{\alpha_0} + \dfrac{(\alpha_3\alpha_0 + \alpha_5\alpha_1)\alpha_1}{\alpha_0^2}}{\alpha_0} \end{aligned}\right\} \tag{A.3}$$

Also, Eq. (11) gives the following relation

$$\frac{\omega(\zeta)}{\omega'(\zeta)}\overline{\phi_0'(\zeta)} = K_3\zeta^3 + K_1\zeta + \mathrm{O}\left(\frac{1}{\zeta}\right) \tag{A.4}$$

in which

$$\left.\begin{aligned} K_1 &= -3\frac{\alpha_5 c_3}{\alpha_0} - \frac{c_1\alpha_3}{\alpha_0} - \frac{c_1\alpha_5\alpha_1}{\alpha_0^2} \\ K_3 &= -\frac{\alpha_5 c_1}{\alpha_0} \end{aligned}\right\} \tag{A.5}$$

Next, by comparing the same powers of the complex variable ζ in Eq. (12) the following linear system of complex algebraic equations is obtained for the computation of the constant coefficients c_1, c_3 and c_5

$$\begin{bmatrix} 1-\frac{\alpha_3}{\alpha_0}-\frac{\alpha_5\alpha_1}{\alpha_0^2} & -3\frac{\alpha_5}{\alpha_0} & 0 \\ -\frac{\alpha_5}{\alpha_0} & 1 & 0 \\ 0 & 0 & 1 \end{bmatrix}\begin{bmatrix} c_1 \\ c_3 \\ c_5 \end{bmatrix} = \begin{bmatrix} -P\alpha_1 - \Gamma'\alpha_0 + \Gamma\alpha_0 b_{-1} \\ -P\alpha_3 + \Gamma\alpha_0 b_1 \\ -P\alpha_5 + \Gamma\alpha_0 b_3 \end{bmatrix} \tag{A.6}$$

The solution of the above system is the following:

$$\begin{aligned} c_1 &= -\frac{\Gamma[\alpha_0(\alpha_1\alpha_0 + 6\alpha_5\alpha_3 + \alpha_1\alpha_3) + \alpha_5\alpha_1(3\alpha_5 + \alpha_1)] + P\alpha_0(\alpha_1\alpha_0 + 3\alpha_5\alpha_3) + \Gamma'\alpha_0^3}{\alpha_0(\alpha_0 - \alpha_3) - \alpha_5(\alpha_1 + 3\alpha_5)} \\ c_3 &= -\frac{\Gamma[\alpha_0(2\alpha_5\alpha_1 + \alpha_3\alpha_0 - \alpha_3^2) + \alpha_5\alpha_3(3\alpha_5 - \alpha_1)] + P[\alpha_0(\alpha_5\alpha_1 + \alpha_3\alpha_0 - \alpha_3^2) - \alpha_3\alpha_5\alpha_1] + \Gamma'\alpha_5\alpha_0^2}{\alpha_0(\alpha_0 - \alpha_3) - \alpha_5(\alpha_1 + 3\alpha_5)} \\ c_5 &= -\Gamma\alpha_5 - P\alpha_5 \end{aligned} \tag{A.7}$$

Finally, the complex functions $\phi(\zeta)$ and $\psi(\zeta)$ can be easily computed by virtue of Eqs. (14) and (15), respectively. Subsequently, the stresses and displacements can be computed by using Eqs. (16).

References

Carranza-Torres, C., Fairhurst, C., 1999. The elastoplastic response of underground excavations in rock masses that satisfy the Hoek–Brown failure criterion. Int. J. Rock Mech. Min. Geomech. Abstr. 36, 777–809.

Cheatham Jr., J.B., 1993. A new hypothesis to explain stability of borehole breakouts. Int. J. Rock Mech. Min. Sci. Geomech. Abstr. 30 (7), 1095–1101.

Exadaktylos, G.E., Stavropoulou, M., 2002. A closed-form elastic solution for stresses and displacements around tunnels. Int. J. Rock Mech. Min. Sci. 39 (7), 905–916.

Gough, D.I., Bell, J.S., 1982. Stress orientations from borehole wall fractures with examples from Colorado, east Texas, and nothern Canada. Can. J. Earth Sci. 19, 1358–1370.

Guisiat, F.D., Haimson, B.C., 1992. Scale effects in rock mass stress measurements. Int. J. Rock Mech. Min. Sci. Geomech. Abstr. 29 (2), 99–117.

Hottman, C.E., Smith, J.H., Purcell, W.R., 1979. Relationship among earth stresses, pore pressure and drilling problems offshore gulf of Alaska. J. Petrol. Technol. 31, 1477–1484.

ITASCA, 1995. Fast Lagrangian analysis of continua. Itasca Consulting Group, Inc., Minnesota.

Jaeger, J.C., Cook, N.G.W., 1976. Fundamentals of rock mechanics, second ed. Chapman and Hall, London, UK.

Kirsch, G., 1898. Die Theorie der Elastizitat und die Bedurfnisse der Festigkeitslehre. Z. Ver. deut. Ing. 42, 797.

Mitchell, L.H., 1966. Stress-concentration factors at a doubly-symmetric hole. The Aeronaut. Quart. 17, 177–186.

Muskhelishvili, N.I., 1963. Some basic problems of the mathematical theory of elasticity. P. Noordhoff Ltd, Groningen, The Netherlands (p. 718).

Neuber, H., 1936. Zur theorie der technischen formzahl. Forsch. a.d. Geb. d. Ing. 7, 271–274.

Novozhilov, V.V., 1961. Theory of Elasticity. Pergamon Press, New York.

Papamichos, E., 2002. Personal communication.
Savin, G.N., 1961. Stress Concentration around Holes. Pergamon Press, Oxford.
Zheng, Z., Cook, N.G.W., Myer, L.R., 1988. Borehole breakout and stress measurements. In: Proceedings of the 29th US Symposium on Rock Mechanics. A.A. Balkema, Rotterdam, pp. 471–478.
Zoback, M.D., Moos, D., Mastin, L.G., Anderson, R.N., 1985. Well-bore breakouts and in situ stress. J. Geophys. Res. 90, 5523–5530.